Direct interpretation of near-field optical images

Alain Dereux, E. Devaux, J. C. Weeber, J. P. Goudonnet, Christian Girard

Revised version submitted to the Proceedings of NFO-6 (Journal of Microscopy)

Direct interpretation of near-field optical images

A. Dereux, E. Devaux, J. C. Weeber, J. P. Goudonnet

Laboratoire de Physique, Optique Submicronique, Université de Bourgogne, BP 47870, F-21078 Dijon, France

C. Girard

Centre d'Elaboration des Matériaux et d'Etudes Structurales (CNRS), BP 4347, F-31055 Toulouse, France

PACS numbers and related keywords:

07.79.Fc: Near-field scanning optical microscopes

73.20.Mf: Plasmons

78.66-w: Optical properties of surfaces, and low-dimensional structures

Corresponding author: A. Dereux (e-mail: adereux@u-bourgogne.fr)

Short title: Interpretation of near-field optical images

December 5, 2000

Abstract. The interpretation of the detection process in near–field optical microscopy is reviewed on the basis of a discussion about the possibility of establishing *direct comparisons* between experimental images and the solutions of Maxwell equations or the electromagnetic local density of states. On the basis of simple physical arguments, it is expected that the solutions of Maxwell equations should agree with images obtained by collecting mode near–field microscopes, while the electromagnetic local density of states should be considered to provide a practical interpretation of illumination mode near–field microscopes.

We review collecting mode near–field microscope images where the conditions to obtain good agreement with the solutions of Maxwell equations have indeed been identified. In this context of collecting mode near–field microscopes, a fundamental different functionality between dielectric and gold coated tips has been clearly identified experimentaly by checking against the solutions of Maxwell equations. It turns out that dielectric tips detect a signal proportional to the optical electric field intensity while gold coated tips detect a signal proportional to the optical magnetic field intensity. The possible implications of this surprising phenomenon are discussed.

1. Introduction

Until now, the development of techniques leading to optical resolution beyond the diffraction limit (also called "optical super–resolution") has somewhat occulted the basic question of the interpretation of the signal detected by near–field optical microscopes (Courjon and Bainier, 1994; Pohl and Courjon, 1993). Obviously, optical super–resolution was expected to make possible the observation of smaller structures than those identified with a standard far–field optical microscope. The interpretations of experimental images often relied on the implicit intuitive assumption that the detected contrasts should allow to recover the exact shapes of the observed material structures. However, as discussed in reference (Hecht *et al.*, 1997), it turns out that many of the cases where this agreement is found are suspected to be related to artefacts due to controlling the tip motion with a feedback loop, not using the near–field optical signal, but using auxiliary AFM (shear–force) or STM signals. Moreover, although rarely mentionned clearly in the literature, this kind of agreement does not show up in many experimental near–field optical images recorded under artefact free conditions.

In this context, the theoretical works aimed at interpreting near–field optical images may adopt one of the two following points of view. The first one intends to recover the exact shapes of the observed material structures by applying mathematical techniques which are akin of inverse scattering and/or deconvolution methods (Garcia and Nieto-Vesperinas, 1993; Carminati and Greffet, 1995; Greffet and Carminati, 1997). This approach still implicitly assumes that near–field optical images should allow to identify the exact shapes of the underlying material structures, albeit after some data processing.

It needs to rely on a calibration step imaging well defined test objects in order to deduce the response function of the nanometer size tips used in near–field optical microscopy. Applying this strategy requires that the same calibrated tip first scans the test object before the sample of interest. Until now, the fragility of most of the commonly used near–field optical probes prevents that the same tip can be systematically used on two successive samples. The practical value of this approach would improve if less fragile tips were available or if the *optical* response function of any given kind of tip was guaranteed to be constant from one tip to the next. The actual state of the art of tips fabrication does not provide such standard.

The second point of view deliberately avoids to discuss about the principle of recovering the exact shapes of the observed material structures (Dereux *et al.*, 2000). Since it takes into account the above mentionned constraints of fragigility and reproductibility of tips, one can regard this point of view as a *practical* alternative to the interpretation of near–field optical images. This approach may also be qualified as "direct" because it does not require any preceding calibration step on a test object but relies on the direct comparison of experimental near-field optical images with the output of Maxwell equations, as obtained by any of the various computational methods which are available today (for a review of these methods, see Girard and Dereux (1996)). This point of view leads to an interpretation of the near–field optical images as maps of the detection in direct space of the physical quantities defined in Maxwell equations. The present paper is devoted to review the current status of this second kind of interpretation, to be refered as "direct". For this purpose, we first summarize what kind of electromagnetic near–fields are known to exist in the vicinity of surfaces.

1.1. Electromagnetic fields close to surfaces

In electrodynamics, a surface is known to support two different classes of localized electromagnetic fields:

(i) Surface electromagnetic fields resulting of an external excitation (like photon or electron beams incident on a surface) are the excited states of the photon field. Since they can be tuned by an external operator, they are involved in the various optical near–field microscope setups.

(ii) Quantum zero point fluctuations of electromagnetic fields confined near a solid–vacuum interface, existing in the absence of any external excitation, are parts of the ground state of the photon field. They are responsible for near–field dispersion effects, such as the van der Waals force field. They are well–known to play a significant rôle in local probe experiments such as Atomic Force Microscopy (Güntherodt and Wiesendanger, 1993; Güntherodt *et al.*, 1995).

The common feature of all scanning probe optical microscopes is the nanometre–sized tip which is piezoelectrically driven to scan close to the sample surface. However, according to the experimental setup (see the review of existing devices by Courjon and Bainier (1994)), the tip may be used as a local source of light or as a local probe. This leads to distinguish the various scanning probe optical microscopes between devices using *illuminating* probe tips and devices using *collecting* probe tips. Among the collecting probe devices, we find the PSTM (Photon Scanning Tunneling Microscope) (Reddick *et al.*, 1989; Courjon *et al.*, 1989) and the family of so–called "apertureless" near–field optical microscopes (Specht *et al.*, 1992; Zenhausern *et al.*, 1994; Zenhausern *et al.*, 1995) which all use their tips as local probes only. PSTM exploits bare and sharply elongated optical fibres which may eventually be coated with metals while apertureless microscopes are using bare metal tips.

The various transmission SNOM (Scanning Near-Field Optical Microscope) (Pohl *et al.*, 1984; Betzig *et al.*, 1986) configurations belong to the category of illuminating probe devices because their probe act as a local emitter of light. Reflection SNOM devices (Fischer *et al.*, 1988) use their tips both as local emitter and local probe, but the discussion below will make clear that they are fundamentally illuminating probe devices. SNOM favor metallized tips with a subwavelength aperture at the apex. Today, they are mostly obtained by coating a sharply elongated optical fibre. Recent alternatives involves tips with a tetrahedral termination (entirely or partly coated with metal) (Koglin *et al.*, 1997) or microfabricated silicon–nitride tips with various shapes and coatings. In fact, as detailed in a recent review, the design of tips is still an open problem (Courjon and Bainier, 1994). It mostly relies on empirical steps. The optimal tip characteristics for ensuring the best imaging properties are not well stated.

When modeling scanning probe optical devices, practical computational reasons require the simplification of the cumbersome task of taking the tip to sample coupling accurately into account. Cases in which the interpretation of scanning probe optical microscope images is problematic are often attributed to the approximations made in describing each kind of tip. This complicates seriously the application of inverse scattering or deconvolution–like methods based on the point of view of recovering the shapes of underlying structures. Instead of refining the description of this coupling, the direct interpretation discussed here avoids to include the tip in the theoretical computations, albeit, as we detail below, it is still based on the distinct features of each family of probe tips.

A measurement aims at providing some information about a physical system. Although quantum physics has revealed that the situation may be complicated by entangled states, relevant information is any describing some aspect of the physical

system, aspect that is still supposed to exist in the absence of the measurement process. With the classification of section 1.1 in mind, let us now consider what kinds of physical quantities do exist, close to a sample surface, at optical frequencies and in the absence of any measurement process, i.e. *if no probe tip is present.* In view of the above distinction, the physical quantities are of different natures according to the collecting or illuminating character of the probe tips.

1.3. Collecting probe tips

In this case, the illumination of the sample is achieved by a classical incident wave. In PSTM setups, the illuminating field is incident below the surface, through a prism on which the sample lies, at an angle larger than the critical angle for total reflexion θ_{tot}. Above a perfectly flat surface, the resulting incident field is a surface wave which decays exponentially along the z direction perpendicular to the surface.

Some apertureless microscopes also use the total internal reflection to excite surface plasmons of thin metal film (Specht *et al.*, 1992; Grésillon *et al.*, 1999). Above a perfectly flat surface, the near–field of the surface plasmon also decays exponentially along the z direction. Other apertureless microscopes (Zenhausern *et al.*, 1994) use the external illumination from the outside medium so that the distribution of the electromagnetic field close to a perfectly flat sample depends on the incident angle. Indeed, except at the Brewster angle, the field intensity is then modulated by the interference between incident and reflected waves.

In the absence of the tip, a common feature of collecting mode devices is thus the well–codified spatial dependence of the incident field illuminating a perfectly flat surface. Such well–defined incident field is scattered by the various structures lying on the sample surface. The total field, resulting from the superposition of the incident and the scattered fields, builds a specific distribution of the electromagnetic near–field. The essential feature of collecting probe devices is that such optical near–fields are excited state of the photon field. They thus belong to the category (i) of the classification introduced in section 1.1. For the practical purpose of the direct interpretation, the optical near–field is described theoretically by solving Maxwell equations *in the absence of the tip*, the incident field being defined by the experimental conditions. The point of view of the direct interpretation brings thus to the fore that the quantities which could be expected to be measured by collecting probe tips are related to those defined in Maxwell equations, namely the electric field and the magnetic field at optical frequencies.

1.4. Illuminating probe tips

In the other group of near–field optical microscopes, the incident field is due to the emitting tip which is assumed to deliver a spatially localized source of light (Betzig

et al., 1992; Fischer and Pohl, 1989; Harootunian *et al.*, 1986; Novotny *et al.*, 1995; Novotny *et al.*, 1997). *In the absence of the tip*, the optical near–fields correspond to the ground state of the photons field, i.e. to the electromagnetic near–fields which exist spontaneously in the absence of any external driving excitation. They thus belong to the category (ii) of the classification of section 1.1. The said quantum fluctuations of the ground state involve all eigenfrequencies of the system (Cohen-Tannoudji *et al.*, 1977) but, in analogy with the procedure followed in STM, only the Fourier component at the frequency ω used in a specific near–field optical experiment turns out to be relevant.

In the case of illuminating probe devices, the point of view of direct interpretation suggests that the quantity which could be expected to be measured is related to the local density of states (LDOS) $\rho(\mathbf{r}, \omega)$ of the electromagnetic field. Since it describes the distribution of the electromagnetic field when there is not any incident field, the LDOS is not a commonly used concept in optics textbooks. A well–known example involving the concept of LDOS is Planck's description of the black body radiation where the LDOS multiplies the Bose–Einstein distribution.

1.5. Direct interpretation of the images

To validate the point of view of direct interpretation, one must find experimental evidence to support positive answers to the following questions:

(a) Are the images recorded by collecting probe devices in agreement with the distributions of the electric and/or magnetic near–fields scattered by the sample surfaces, as computed without including any tip?

(b) Is there any link between the images obtained by illuminating probe devices and the ω-resolved distribution of the electromagnetic local density of states $\rho(\mathbf{r}, \omega)$ close to the sample surface, as computed without including any tip?

The section 3 below reviews recent experimental results which lead to answer positively to the point (a). To our knowledge, although the relevance of the LDOS as been assessed theoretically (Dereux *et al.*, 2000), the works analyzing the experimental images of illuminating probe devices have not yet tried to find any agreement with the LDOS. Therefore, the status of point (b) should be understood as a suggestion aimed at finding an issue to the difficult problem of the interpretation of the images obtained with illuminating probe devices.

2. Theoretical principles

The practical point of view of direct interpretation proposed in section 1 requires a single theoretical framework which enables, close to the sample surface, the computation of the

scattering of th electric and magnetic fields in the case of collecting probe devices and a description of the LDOS in the case of illuminating probe devices. These both features are delivered by a formulation based on the use of Green dyadics, or propagators, which we summarize in this section(Girard and Dereux, 1996).

2.1. Scattering theory

With the usual $\exp(-i\omega t)$ time (t) dependence, $\mathbf{r}$ being a vector in direct space and ω being the angular frequency, the vector wave equation issued from Maxwell's equations (SI units: $c = \sqrt{\epsilon_0\ \mu_0}$ is the speed of light in vacuum):

$$-\nabla \times \nabla \times \mathbf{E}(\mathbf{r},\omega) + \frac{\omega^2}{c^2}\,\epsilon(\mathbf{r},\omega)\,\mathbf{E}(\mathbf{r},\omega) = 0 \tag{1}$$

may be cast as

$$-\nabla \times \nabla \times \mathbf{E}(\mathbf{r},\omega) + q^2\ \mathbf{E}(\mathbf{r},\omega) = \mathbf{V}(\mathbf{r},\omega)\ \mathbf{E}(\mathbf{r},\omega) \tag{2}$$

with

$$q^2 = \frac{\omega^2}{c^2}\,\epsilon_{ref}\,. \tag{3}$$

Any complicated behavior due the anisotropy or to the low-symmetry of the geometrical shape of the original dielectric tensor profile $\epsilon(\mathbf{r},\omega)$ is described as a difference relatively to the reference system ϵ_{ref} ($\mathbf{1}$ is the unit dyadic):

$$\mathbf{V}(\mathbf{r},\omega) = \frac{\omega^2}{c^2}\ \left(\mathbf{1}\ \epsilon_{ref} - \epsilon(\mathbf{r},\omega)\right). \tag{4}$$

The implicit Lippmann-Schwinger equation provides a solution of equation (2):

$$\begin{aligned}\mathbf{E}(\mathbf{r},\omega) &= \mathbf{E}_0(\mathbf{r},\omega)\\ &+ \int_V d\mathbf{r}^{'}\ \mathbf{G}_0(\mathbf{r},\mathbf{r}^{'},\omega)\ \cdot \mathbf{V}(\mathbf{r}^{'},\omega)\cdot\ \mathbf{E}(\mathbf{r}^{'},\omega).\end{aligned} \tag{5}$$

In scattering theory, the first term $\mathbf{E}_0(\mathbf{r},\omega)$ is refered as the incident field while the second term is called the scattered field obtained from the integration over the domain V where $\mathbf{V}(\mathbf{r}^{'},\omega)$ is non-zero. V defines the volume of the scatterer relatively to the reference system. This last equation can easily be solved numerically so that it provides a useful tool for the evaluation of the theoretical distributions of the electric field in the near zone.

To solve the Lippmann–Schwinger equation, we need to know the analytical solution $\mathbf{E}_0(\mathbf{r},\omega)$ satisfying

$$-\nabla \times \nabla \times \mathbf{E}_0(\mathbf{r},\omega) + q^2\ \mathbf{E}_0(\mathbf{r},\omega) = 0 \tag{6}$$

and the associated Green's dyadic defined by

$$\begin{aligned}-\nabla \times \nabla \times \mathbf{G}_0(\mathbf{r},\mathbf{r}^{'},\omega) + q^2\ \mathbf{G}_0(\mathbf{r},\mathbf{r}^{'},\omega)&\\ = \mathbf{1}\ \delta(\mathbf{r}-\mathbf{r}^{'})&\end{aligned} \tag{7}$$

where $\delta(\mathbf{r}-\mathbf{r}^{'})$ is the Dirac delta function. The reference structure ϵ_{ref} is usually a homogeneous background material or a semi-infinite surface system so that $\mathbf{E}_0(\mathbf{r},\omega)$ is known analytically. For homogeneous media, the analytical form of $\mathbf{G}_0(\mathbf{r},\mathbf{r}^{'},\omega)$ is known from ancient works (Morse and Feshbach, 1953; Levine and Schwinger, 1950). For a surface system, the expression of the propagator is somewhat more elaborated but is also found in the literature (Girard and Bouju, 1992; Paulus *et al.*, 2000).

Once the electric field has been determined, the magnetic field $\mathbf{H}(\mathbf{r},\omega)$ is deduced trough an integral equation involving the mixed propagator $\mathbf{Q}_0(\mathbf{r},\mathbf{r}^{'},\omega)$ (see details in Girard *et al.* (1997)):

$$\begin{aligned}\mathbf{H}(\mathbf{r},\omega) &= \mathbf{H}_0(\mathbf{r},\omega) \\ &+ \frac{1}{\mu_0 c}\int_V d\mathbf{r}^{'}\ \mathbf{Q}_0(\mathbf{r},\mathbf{r}^{'},\omega)\cdot\mathbf{V}(\mathbf{r}^{'},\omega)\cdot\mathbf{E}(\mathbf{r}^{'},\omega)\end{aligned} \tag{8}$$

2.2. Local density of states

Well–known in solid state physics (Economou, 1983), the use of the LDOS is not commonly spread in electrodynamics (Agarwal, 1975; Martin *et al.*, 1999). Solid state physics applies the concept of LDOS to non–relativistic electrons so that the LDOS corresponds to the density of probability to find an electron of energy $\hbar\omega$ at the point $\mathbf{r}$ of the solid. This function is directly related to the square moduli of all possible electronic wavefunctions associated to this energy. In the case of photons, different formulations of the LDOS can be proposed depending on the reference field (electric or magnetic). The most widely used formulation relies on the calculation of the electric field susceptibility The LDOS is then deduced from the electric Green's dyadic $\mathbf{G}(\mathbf{r},\mathbf{r}^{'},\omega)$ of a sytem

$$\rho(\mathbf{r},\omega) = -\frac{1}{\pi}\,\Im\, Trace\ \mathbf{G}(\mathbf{r},\mathbf{r},\omega) \tag{9}$$

where $\Im$ denotes the imaginary part. The vector character of electromagnetic fields allows to view this LDOS as the sum

$$\rho(\mathbf{r},\omega) = \sum_{j=x,y,z}\rho_{jj}(\mathbf{r},\omega) \tag{10}$$

where the "partial" LDOS are defined by:

$$\rho_{jj}(\mathbf{r},\omega) = -\frac{1}{\pi}\,\Im\,\mathbf{G}_{jj}(\mathbf{r},\mathbf{r},\omega). \tag{11}$$

With this reference field, the LDOS is related to the square moduli of the electric field associated to all electromagnetic *eigenmodes* of frequency ω. When this quantity is defined on the basis of any kind of mixed field–susceptibilities, such straightforward relation to the electric field is not possible anymore. However, in any case, the LDOS is the only quantitative way to describe the *continuous* part of the spectrum of any

system independently of the excitation mode. In the context of optics, this means that the LDOS provides spectroscopic informations which are intrinsically independent of any particular illumination mode. This independence is exactly the basic feature which is postulated in the practical point of view of the direct interpretation.

Within the framework of the linear response theory, the propagator entering equation (9) is a second rank tensor which verifies a dyadic Dyson equation:

$$\mathbf{G}(\mathbf{r},\mathbf{r}^{'},\omega) = \mathbf{G}_0(\mathbf{r},\mathbf{r}^{'},\omega) + \int_V \mathbf{G}_0(\mathbf{r},\mathbf{r}^{''},\omega)\cdot\mathbf{V}(\mathbf{r}^{''},\omega)\cdot\mathbf{G}(\mathbf{r}^{''},\mathbf{r}^{'},\omega)\,d\mathbf{r}^{''}\,, \tag{12}$$

so that it may be deduced using the propagator $\mathbf{G}_0(\mathbf{r},\mathbf{r}^{'},\omega)$ of a reference system (homogeneous medium or surface) that we defined above (Girard *et al.*, 1993; Girard *et al.*, 1994; Martin *et al.*, 1995).

Since the propagator $\mathbf{G}(\mathbf{r},\mathbf{r}^{'},\omega)$ provides the value of the electric field at an observation point $\mathbf{r}$ due to a point–like dipolar source located at $\mathbf{r}'$, one can view that a given partial LDOS corresponds to a specific orientation of the point dipolar source. The point of view of direct interpretation brings to the fore that comparing the images recorded by an illuminating probe device, equiped with a specific tip, to the LDOS (or to any well–suited combination of partial LDOS) could provide a figure of merit of how the said probe tip is akin of a point source of light. As mentionned above, checking experimental images against LDOS maps has not yet been undertaken. We therefore limit the discussion to what kind of results might be expected.

A rapid overview of the near–field optics literature brings easily to the fore that the ideal active probe device is considered to be a point-like source of light. Various empirical procedures intend to produce tips which are as close as possible to this ideal emitting feature. A fluorescing structure (made of one or several molecules) attached at the apex of a tip provides a good approximation to such ideal point source. Dereux *et al.* (2000) performed a theoretical assessment of the relevance of the electromagnetic LDOS to interpret the images delivered by illuminating probe devices using the model of a fluorescent structure as local emitter of light: on the basis of some simplifying assumptions about the symmetry properties of the molecule (supposed to belong to the $C_{\infty v}$ symmetry group) and about the modeling of its polarizability (assumed to the one of a two level system), it turns out that the spontaneous molecular decay rate is modified by any changes in the electromagnetic local density of states with respect to LDOS of vacuum (implicitly contained in the natural linewidth Γ_0). The average effective line width $\Gamma(\mathbf{r}_m)$ is then found to be (ω_0 being the fluorescence frequency)

$$\Gamma(\mathbf{r}_m) = \Gamma_0 + \frac{\pi\omega_0^2 A_0}{c^2}\rho(\mathbf{r}_m,\omega_0), \tag{13}$$

where $\rho(\mathbf{r}_m,\omega_0)$ (the LDOS computed at the location $\mathbf{r}_m$ of the molecule) has been defined in equation (9) and where A_0 is the oscillator strength associated to the transition

between the two quantum levels of the model system.

Within the above mentionned approximations, the spontaneous molecular decay rate is related to the LDOS as given by performing the full trace of the propagator, i.e. by considering a point source where all orientations are involved with equal weights. When trying to match the images recorded with other kinds of local sources (molecules with other symmetry properties, tetrahedral tips, apertures,...), one could find that some other combination of the partial LDOS's might be better suited.

At a given position, a larger LDOS, which means that a growing number of electromagnetic states are available, is responsible for shorter lifetime of the molecule. Let us now imagine that the fluorescent structure scans a sample surface. Referring to the classification of illuminating probe devices introduced in section 1, such structure may be viewed as an ideal point source. According to equation (13), scanning a fluorescent structure should image the electromagnetic LDOS. To illustrate what kind of information can then be extracted from $\Gamma(\mathbf{r}_m)$, figure 1 presents LDOS maps close to a system of nanoscopic glass pads deposited on a flat glass surface. The symmetry of the pads arrangement builds a specific LDOS pattern where maxima may occur at other locations than right above the pads (figure 1 (B)). One can then expect that an illuminating probe device provides an image which does not allow a direct recognition of the shape of the underlying objects. Indeed, as in the exemple of figure 1, the LDOS and the partial LDOS's may display significant discrepancies relatively to the shapes of the underlying objects.

3. Comparison of theoretical and experimental images: the case of collecting probes

The point of view of direct interpretation states that images recorded by collecting probe devices should be interpreted as the result of the scattering of quasi–two–dimensional surface waves by the various defects (asperities, kinks, holes, etc...) lying on the sample surface. The surface waves generated by total internal reflection are viewed as quasi–two–dimensional because they decay exponentially in the direction normal to the sample surface. The structures deposited on, or buried in, the surface scatter these waves parallel to the surface and induce some loss due to diffraction which couples light to the external medium. Collecting probe near–field optical microscopes approach a local probe very close to the sample surface so that they detect mostly the field distribution of the quasi–two–dimensional scattered surface wave rather than the diffracted components which propagate away from the sample surface. In the case of a collecting probe device, this section provides evidence that one can match experimental images with theoretical maps of the distributions of quantities defined in Maxwell equations, namely the electric and magnetic fields at optical frequencies.

3.1. Experimental setup and test sample

The basic experimental setup is a D3000 scanning force microscope (Digital Instruments). With the cantilever replaced by a sharpened optical fibre tip, it is used as a PSTM (Reddick *et al.*, 1989) operating in constant height mode. The tip, which may be either bare or (subsequently) coated with a thin film of Au, is piezoelectrically driven to scan close to the sample surface. The sample, deposited upon a glass prism, is illuminated in total internal reflection (angle of incidence $\theta = 60$ degrees) by either a red laser (wavelength in vacuum $\lambda = 633$ nm) or by a green laser ($\lambda = 543$ nm). A polarizer is placed between the laser and the prism. The azimuthal angle ψ, describing the orientation of the incident surface wave wavevector around the z axis, has a value close to 90 degrees (with reference to the x axis lying in the plane of the sample surface (see figures 2,3 and 5)) which is not precisely controlled since it depends on the orientation of the sample on the prism.

Fig.2 (a) shows the topography, recorded by atomic force microscopy, of a typical dielectric pattern used as a reference sample. Seven glass pads were formed on a glass substrate by a nanofabrication process based on electron beam lithography. Their lateral size is about 130 nm and their height is about 100 nm. The closest distance between two pads is 900 nm. The 7-pads pattern is reproduced every 20 μm along horizontal lines on the sample surface. The glass substrate has the same index of refraction as the prism on which it lies.

In constant height mode, the gray scales of the 512×512 PSTM images (Fig 2 (b,c,d) and Fig. 5) depict the variations of the detected intensity. Due to the weak power of our green laser, the images recorded at $\lambda = 543$ nm with coated tips were somewhat noisy. The Savitzky-Golay algorithm filtered this noise by introducing a minimal broadening (Press *et al.*, 1986). Successive constant height scans were performed upon approaching the tip to the sample by 10 nm steps. The PSTM images presented here have been recorded at the last setpoint which allowed scanning without crashing into any of the pads: the constant heights of the scans are therefore presumably a few nanometers above the pads.

The local probes are multimodes fibres sharpened by heating and pulling. The resulting tips look like cones with small aperture angles (< 20 degrees), terminated by rounded apexes with radii between 20 and 50 nm. The mean radius of the part of the tip which is in the decay range of the evanescent wave is about 80 nm. After the pulling, the fibre may eventually be fully coated (no resulting aperture) with a metal while turning around its axis in a calibrated evaporator.

3.2. Theoretical maps of the electric and magnetic fields

To obtain the theoretical distributions of $|\mathbf{E}(\mathbf{r})|^2$ and of $|\mathbf{H}(\mathbf{r})|^2$ (Fig.3), the topography of Fig.2 (a) is used as input data of a program based on the Green dyadic method summarized in the preceding section 2. The data are discretized by $30 \times 30 \times 30$ nm^3 cubes and the incident wave conforms to the experimental conditions. The intensity is calculated in a plane at a constant height z_{ref} above the sample surface. It is then normalized to the intensity at the same height when no pads lie on the surface. According to a procedure reported recently (Krenn *et al.*, 1999a), the value of z_{ref} was set to 130 nm, i.e. 30 nm above the top of the pads. Following the principle of the direct interpretation, the theoretical distributions do not include the tip so as to correspond to images due to a pointlike detector. In the experiments, the finite size of the tip broadens the signals above the pads and smooths the surface wave interference patterns. Moreover, the multiple scattering, due to the various defects which are randomly spread on the actual sample surface outside the observation area, attenuates (at least) or modifies into speckle the pronounced interference patterns showing up in the theoretical map because the computations assumed a perfectly flat surface outside the calculation window. The most reliable near–field characteristics are thus the near–field contrasts directly above the pads. The white squares in Fig.3 are the projections of the lower pad showing that, directly above a pad, $|\mathbf{E}(\mathbf{r})|^2$ produces a bright contrast (Fig.3 (a)) while $|\mathbf{H}(\mathbf{r})|^2$ is characterized by a dark contrast surrounded by two bright lobes (Fig.3 (b)) as explained in references (Girard *et al.*, 1997; Girard *et al.*, 1998).

3.3. Detecting the electric field

Using *p*-polarized incident beams, Fig.2 (b) and (d) show typical PSTM images recorded when observing the reference sample with bare dielectric (uncoated) optical fibre tips at both green and red wavelengths. The arrows indicate the positions where the tips crashed into the pads in the subsequent constant height images, performed less than 10 nm closer to the sample. This procedure ensures that a bright contrast is detected in juxtaposition with the glass pads, which is in agreement with a calculation of the distribution of $|\mathbf{E}(\mathbf{r})|^2$ close to the sample surface (Fig.3 (a)). Previous works on the same kind of sample have demonstrated that the agreement of PSTM images with theoretical distributions of $|\mathbf{E}(\mathbf{r})|^2$, as computed without including the tip, still holds when considering the dependence upon the incident polarization (Girard *et al.*, 1998; Girard *et al.*, 1995; Weeber *et al.*, 1996). Also, still using bare dielectric optical fibre tips, constant height PSTM images performed close to metallic nanoparticles of about the same size as the dielectric pads of Fig.2 (a) turned out to agree perfectly well with theoretical distributions of the electric field intensity, as computed without including the tip (Krenn *et al.*, 1999a).

3.4. Detecting the magnetic field

Although Maxwell equations state that an optical wave is of electro–magnetic nature, optical signals are usually found to be proportional only to the intensity of the *electric* field associated with the optical wave. As stated above, this proportionality has also been found to be valid in constant height PSTM images recorded with bare dielectric optical fibre tips.

The detection of a signal proportional to the intensity of the *magnetic* field $|\mathbf{H}(\mathbf{r})|^2$ associated with an electromagnetic wave is a well–known phenomenon at very low frequencies. At very low frequencies, the required dimensions of a metal loop where the incident magnetic field induces an electric current are indeed sufficiently large for it to be easily fabricated. Applying this detection scheme to optical frequencies requires loops with radii smaller than 200 nm, made of metals which can sustain collective oscillations of the conduction electron gas relative to a background of positive charges. At optical frequencies, noble metals, like Ag or Au, are well-known to sustain such oscillations which are refered to as plasmons modes. One can then imagine that a nanoscopic metal loop, resulting from the coating of a sharpened optical fibre with a noble metal, may be sensitive to the magnetic part of a wave oscillating at optical frequencies.

However, in the above mentioned range of radii, it is well established that the optical properties of small metal structures are governed by localized surface plasmon (LSP) modes which are very sensitive to geometrical parameters like shape and size (Boardman, 1982). In order to find, at the frequency of the laser operated in the experiment, the correct thickness of the coating which can sustain a circular symmetry plasmon, we considered the simple model of a dielectric cylinder covered by a thin metal coating. Following a standard procedure (Kliewer and Fuchs, 1974; Pfeiffer *et al.*, 1974) and assuming a Au coating of thickness d surrounding a glass core of radius b, we searched for the plasmon modes. These are characterized by fields that are exponentially decreasing for radial coordinates larger than $a = b+d$, oscillatory along the longitudinal axis of the cylinder and have an $e^{im\phi}$ angular dependence. Their dispersion relation depends implicitly on the ratio a/b. We considered only the $m = 1$ plasmon modes since the incident photons carry unit spins which are exchanged in interactions of light with matter. On the basis of tabulated values of the dielectric function of Au (Palik, 1985) and of the value 2.25 for the dielectric constant of glass, solving the dispersion relation reveals that $m = 1$ plasmon modes may be excited by *visible* incident frequencies for several ratios a/b. Fig.4 depicts such dispersion curves for ratios that will turn out to be pertinent below. The set of dielectric function data of Au was successfully used in reference (Krenn *et al.*, 1999b) to *predict* the occurence of plasmon resonances of nanoscopic structures (nanowires and nanodots deposited on glass) which were then observed experimentally at the right wavelength and at the right location with a PSTM.

Examining the dispersion relation of Fig.4, we notice that, for $a/b = 1.3$, which sets $a = 100$ nm and $d = 23$ nm (point A in Fig.4), a plasmon may be excited by the red laser frequency, but the values of a and d obtained for the green laser do not conform to the actual dimensions of the tips. Since, as discussed above, the typical radius b of the uncoated tips is around 80 nm, tips were coated with 20 nm of Au in order to study the possible influence of a circular symmetry plasmon on the detection process. Indeed, using such coated tips, the nature of the PSTM images turned out to be dependent on the free–space laser wavelength. At $\lambda = 543$ nm (Fig.5 (b)), the PSTM image is quite similar to those recorded with bare dielectric tips (Fig.2 (b) and (d)), i.e, displaying a pattern proportional to $|\mathbf{E}(\mathbf{r})|^2$. However, at $\lambda = 633$ nm (Fig.5 (a)), the PSTM image does not agree with the theoretical distribution of $|\mathbf{E}(\mathbf{r})|^2$ anymore but is found to be proportional to the theoretical distribution of $|\mathbf{H}(\mathbf{r})|^2$ (Fig.3 (b)), as computed without uncluding the tip. We checked that a theoretical distribution obtained by a linear superposition with equal weights of both electric and magnetic fields do not lead to the contrasts observed experimentally. With the same red laser, during the next scan, 10 nm closer to the sample, we noticed that the tip crashed into the lower pad. Specifically, it struck the dark zone between the two bright lobes (arrow in Fig.5 (a)), which is in exact agreement with the actual position of the pad, indicated by the white square, in the calculation of Fig.3(b). Experimentally, we found the surprising new result that the detection of the optical magnetic field with gold coated tips is equally efficient as the detection of the optical electric field with bare dielectric tips provided that the conditions of plasmon excitation are satisfied.

To check the dependence of this phenomenon on the circular symmetry of the coating, we have tested "semi-coated" tips, featuring a dissymmetric Au layer on the dielectric core. The pulled fibre tips are not rotated in the evaporator, while the deposition time is reduced in order to coat only one side with 20 nm of Au. A typical PSTM image recorded with such a tip at $\lambda = 633$ nm appears in Fig.2 (c) and turns out to be proportional to $|\mathbf{E}(\mathbf{r})|^2$, like the images recorded by uncoated tips.

To confirm the role of circular symmetry plasmons in detecting a magnetic signal with a PSTM, we tried to reproduce the phenomenon at the wavelength $\lambda = 543$ nm. We thus searched for the ratio a/b providing a value of b which is not too far from the mean radius of the bare optical fibre apexes. According to the dispersion curves of Fig.4, we chose $a/b = 1.4$ which led to $a = 96$ nm and $d = 29$ nm (point B in Fig.4). We therefore fabricated tips coated with 30 nm of Au which, using the green laser, produce a PSTM image (Fig.5 (c)) characteristic of the distribution of $|\mathbf{H}(\mathbf{r}, \omega)|^2$. We finally fabricated tips coated with 35 nm of Au. Still using the green laser, these tips lead to bright contrasts above the pads (Fig.5 (d)), similar to the images obtained with an uncoated tip. The role of circular symmetry plasmons is thus crucial in the detection of a signal proportional to $|\mathbf{H}(\mathbf{r})|^2$. Indeed, the detection of $|\mathbf{H}(\mathbf{r})|^2$ occurs for parameters (coating

thickness and incident wavelength) related to the dispersion relation of such plasmons. Also, the use of semi-coated tips demonstrated that breaking the fundamental circular symmetry prevents the observation of the phenomenon.

For the sake of brevity, we presented only images obtained with p-polarized incident light. Of course, we also repeated all the above described measurements in s polarization. Even if the contrasts are inverted relative to the p polarization, (Weeber *et al.*, 1996; Girard *et al.*, 1997; Girard *et al.*, 1998; Girard *et al.*, 1995) the results pertaining to the s polarization lead to the same conclusions about the electric or magnetic natures of the detected signals as a function of wavelengths and tip coating thicknesses.

We also considered an alternative interpretation of the images which relies on the hypothesis of the detection of the plasmon field by the objects lying on the surface. Such phenomenon has been reported previously in the context of fluorescence near–field optical microscopy where it turned out that a fluorescing molecule lying on a surface can map the electric field distribution of a non-resonating tip(Betzig and Chichester, 1993). In the circumstances described here, such phenomenon can be discarded on the basis of the above mentionned polarization dependence and on the fact that the pads lying on the surface are of the same order of magnitude as the apex of the tip. Moreover, recent results (to be published elsewhere (Devaux, 2000)), have confirmed that, using optical fibre tips coated exactly as explained above, constant height PSTM images performed close to metallic nanoparticles of about the same size as the dielectric pads of Fig.2 (a) turned out to agree perfectly well with theoretical distributions of the magnetic field intensity, as computed without including the tip.

3.5. Commutation relations between electric and magnetic field components

This section has provided the experimental evidences to support the point of view of the direct interpretation of PSTM images. One can find conditions: suitable design of the probe tip, constant height scanning, definition of an effective height of detection z_{ref}, such that the experimental images agree with the theoretical distributions of either the electric or the magnetic field intensity. Conversely, the point of view of the direct interpretation allows to identify a striking experimental fact: either the electric *or* the magnetic field intensity (not any mixture of both signals) is detected. Switching between both detection modes is achieved by increasing the coating thickness of only 5 nm (see Fig.5 (c) and (d)). Such thickness difference being in the range of the roughness of thin metal films fabricated by vapour deposition, one may wonder how the resulting coated tip operates such exclusive measurement.

At this point, it is interesting to remember the commutation relations between electric and magnetic field components, deduced in the framework of quantum electrodynamics. The $\mathbf{e}_j$, with $j = 1, 2$ and 3, being the unit vectors in Cartesian

coordinates, we first define

$$\mathbf{r} = \sum_{j=1}^{3} x_j \, \mathbf{e}_j \tag{14}$$

$$\mathbf{E}(\mathbf{r}, t) = \sum_{j=1}^{3} E_j(\mathbf{r}, t) \, \mathbf{e}_i \tag{15}$$

$$\mathbf{H}(\mathbf{r}, t) = \sum_{j=1}^{3} H_j(\mathbf{r}, t) \, \mathbf{e}_j \tag{16}$$

In the specific case of harmonic time dependence, the said commutation relations read (h being the Planck constant) (Scully and Zubairy, 1997):

$$[E_l(\mathbf{r}, t), H_m(\mathbf{r}^{'}, t)] = -\frac{ihc^2}{2\pi} \frac{\partial}{\partial n} \delta(\mathbf{r} - \mathbf{r}^{'}) \tag{17}$$

where l, m and n form a cyclic permutation of x_1, x_2 and x_3. These commutation relations state that the parallel components of the electric and magnetic field may be measured simultaneously † whereas the perpendicular components cannot. An interesting feature of these relations is the Dirac delta function $\delta(\mathbf{r} - \mathbf{r}^{'})$ which points out that the reciprocal influence of both measurements shows up only if one intends to perform the simultaneous measurements within the same infinitesimal volume. From the point of view of the direct interpretation, performing measurements within an infinitesimal volume appears to be precisely the core of near-field optical microscopy.

The experimental results thus call for deeper studies in order to determine whether the commutation relations between electric and magnetic field components might be involved in the surprising phenomenon of magnetic field detection. Answering to this question is interesting not only from a theoretical point of view but may also determine the future technical development of near–field optics. Indeed, one important implication deals with the possibility of defining near-field optical devices which would play a role equivalent to the polarizers in standard far–field optics. Up to know, such near-field optical devices are not available. Since the typical feature of far–field optics polarizer is to perform exclusive measurements (i.e. measuring one polarization prevents to find subsequently the light in another polarization state), exclusive measurements of the electric and magnetic field could evolve as the substitute to the polarizers in the near–field zone.

4. Conclusion

This paper discusses the practical point of view of direct interpretation which, according to the collecting and illuminating character of the probe tip, leads to formulate different

† In quantum physics, a "simultaneous measurement" does not refer to a "measurement at the same time", but refers to the reciprocal influence of the two measurements.

hypothesis about the nature of the information contained in near–field optical images. The practical point of view suggests that the distribution of the electric or magnetic near–field scattered by the sample surface is probed by collecting probe devices while the electromagnetic local density of states might be the key to understand the images recorded by illuminating probe devices. In the case of collecting probe devices, the direct comparison of experimental and theoretical results supports the proposed point of view and allows to bring to the fore some interesting implication. The same kind of procedure has not yet been applied to establish whether images recorded with illuminating probe devices should be interpreted on the basis of the ω-resolved electromagnetic LDOS or not.

Acknowledgments

Stimulating discussions and/or collaborations with F. R. Aussenegg, J. R. Krenn, A. Leitner, G. Schider, U. Ch. Fischer, T. L. Ferrell, E. Bourillot, T. David and C. Chicanne are gratefully acknowledged. One of us (A. D.) acknowledges the financial supports of the Regional Council of Burgundy and of the French Ministry for Education and Research.

References

Agarwal, G. S. (1975). *Phys. Rev. A* **11**, 230–242.

Betzig, E. and Chichester, R. J. (1993). *Science* **262**, 1422–1425.

Betzig, E., Finn, P. L., and Weiner, S. J. (1992). *Appl. Phys. Lett.* **60**, 2484.

Betzig, E., Harootunian, A., Lewis, A., and Isaacson, M. (1986). *Appl. Opt.* **25**, 1890–1900.

Boardman, A. D., editor (1982). *Electromagnetic surface modes*, New York. Wiley.

Carminati, R. and Greffet, J. J. (1995). *Opt. Comm.* **1995**, 316.

Cohen-Tannoudji, C., Diu, B., and Laloë, F. (1977). *Mécanique quantique*. Hermann, Paris.

Courjon, D. and Bainier, C. (1994). *Rep. Prog. Phys.* **57**, 989–1028.

Courjon, D., Sarayedine, K., and Spajer, M. (1989). *Opt. Comm.* **71**, 23–28.

Dereux, A., Girard, C., and Weeber, J. C. (2000). *J. Chem. Phys.* **112**, 7775–7790.

Devaux, E. (2000). PhD thesis, Université de Bourgogne, Dijon.

Economou, E. (1983). *Green's functions in quantum physics*, volume 7 of *Springer Series in Solid–State Science*. Springer, Berlin, second edition.

Fischer, U. and Pohl, D. (1989). *Phys. Rev. Lett.* **62**, 458–461.

Fischer, U. C., Dürig, U. T., and Pohl, D. W. (1988). *Appl. Phys. Lett.* **52**, 249–251.

Garcia, N. and Nieto-Vesperinas, M. (1993). *Opt. Lett.* **18**, 2090.

Girard, C. and Bouju, X. (1992). *J. Opt. Soc. Am. B* **9**, 298–305.

Girard, C. and Dereux, A. (1996). *Rep. Prog. Phys.* **59**, 657–699.

Girard, C., Dereux, A., and Martin, O. J. F. (1993). *Surf. Sc.* **295**, 445–456.

Girard, C., Dereux, A., Martin, O. J. F., and Devel, M. (1994). *Phys. Rev. B* **50**, 14467–14473.

Girard, C., Dereux, A., Martin, O. J. F., and Devel, M. (1995). *Phys. Rev. B* **52**, 2889–2898.

Girard, C., Dereux, A., and Weeber, J. C. (1998). *Phys. Rev. E* **58**, 1081–1085.

Girard, C., Weeber, J. C., Dereux, A., Martin, O. J. F., and Goudonnet, J. P. (1997). *Phys. Rev. B* **55**, 16487–16497.

Greffet, J. J. and Carminati, R. (1997). *Prog. Surf. Sci.* **56**, 133–237.

Grésillon, S., Aigouy, L., Boccara, C. A., Rivoal, J. C., Quelin, X., Desmarest, C., Gadenne, P., Shubin, V. A., Sarychev, A. K., and Shalaev, V. M. (1999). *Phys. Rev. Lett.* **82**, 4520.

Güntherodt, H.-J., Anselmetti, D., and Meyer, E., editors (1995). *Forces in Scanning Probe Methods*, volume E 286 of *NATO ASI*, Dordrecht. NATO, Kluwer.

Güntherodt, H.-J. and Wiesendanger, R. (1993). *Theory of Scanning Tunneling Microscopy and related Methods*. Springer Series in Surface Science. Springer, Berlin.

Harootunian, A., Betzig, E., Isaacson, M., and Lewis, A. (1986). *Appl. Phys. Lett.* **49**, 674–676.

Hecht, B., Bielefeldt, H., Novotny, L., Inoue, Y., and Pohl, D. W. (1997). *J. Appl. Phys* **81**, 2492.

Kliewer, K. L. and Fuchs, R. (1974). *Advances in Chemical Physics* **27**, 355–541.

Koglin, J., Fischer, U. C., and Fuchs, H. (1997). *Phys. Rev. B* **55**, 249.

Krenn, J. R., Dereux, A., Weeber, J. C., Bourillot, E., Lacroute, Y., Goudonnet, J. P., Schider, G., Gotschy, W., Leitner, A., Aussenegg, F. R., and Girard, C. (1999a). *Phys. Rev. Lett.* **82**, 2590–2593.

Krenn, J. R., Weeber, J. C., Bourillot, E., Dereux, A., Goudonnet, J. P., Schider, G., Leitner, A., Aussenegg, F. R., and Girard, C. (1999b). *Phys. Rev. B* **60**, 5029–5033.

Levine, H. and Schwinger, J. (1950). *Comm. Pure App. Math.* **3**, 355–391.

Martin, O. J. F., Girard, C., and Dereux, A. (1995). *Phys. Rev. Lett.* **74**, 526–529.

Martin, O. J. F., Girard, C., Smith, D. R., and Schultz, S. (1999). *Phys. Rev. Lett.* **82**, 315.

Morse, P. and Feshbach, H. (1953). *Methods of theoretical physics.* McGraw–Hill, New–York.

Novotny, L., Hecht, B., and Pohl, D. (1997). *J. Appl. Phys.* **81**, 1798.

Novotny, L., Pohl, D., and Regli, P. (1995). *Ultramicroscopy* **11**, 1768.

Palik, E. D. (1985). *Handbook of Optical Constants of Solids.* Academic, San Diego, CA.

Paulus, M., Gay-Balmaz, P., and Martin, O. J. F. (2000). *Phys. Rev. E* **62**. to be published.

Pfeiffer, C. A., Economou, E. N., and Ngai, K. L. (1974). *Phys. Rev. B* **10**, 3038.

Pohl, D. and Courjon, D., editors (1993). *Near-field optics*, volume E 242 of *NATO ASI*, Dordrecht. NATO, Kluwer.

Pohl, D. W., Denk, W., and Lanz, M. (1984). *Appl. Phys. Lett.* **44**, 651–653.

Press, W., Flannery, B., Teukolsky, S., and Vetterling, W. (1986). *Numerical recipes - The art of scientific computing.* Cambridge University Press, Cambridge.

Reddick, R. C., Warmack, R. J., and Ferrell, T. L. (1989). *Phys. Rev. B* **39**, 767–770.

Scully, M. O. and Zubairy, M. S. (1997). *Quantum optics.* Cambrigde.

Specht, M., Pedarnig, J. D., Heckl, W. M., and Hänsch, T. W. (1992). *Phys. Rev. Lett.* **68**, 476–479.

Weeber, J. C., Bourillot, E., Dereux, A., Goudonnet, J. P., Chen, Y., and Girard, C. (1996). *Phys. Rev. Lett.* **77**, 5332–5335.

Zenhausern, F., Martin, Y., and Wickramasinghe, H. K. (1995). *Science* **269**, 1083.

Zenhausern, F., O'Boyle, M. P., and Wickramasinghe, H. K. (1994). *Appl. Phys Lett.* **65**, 1623–1625.

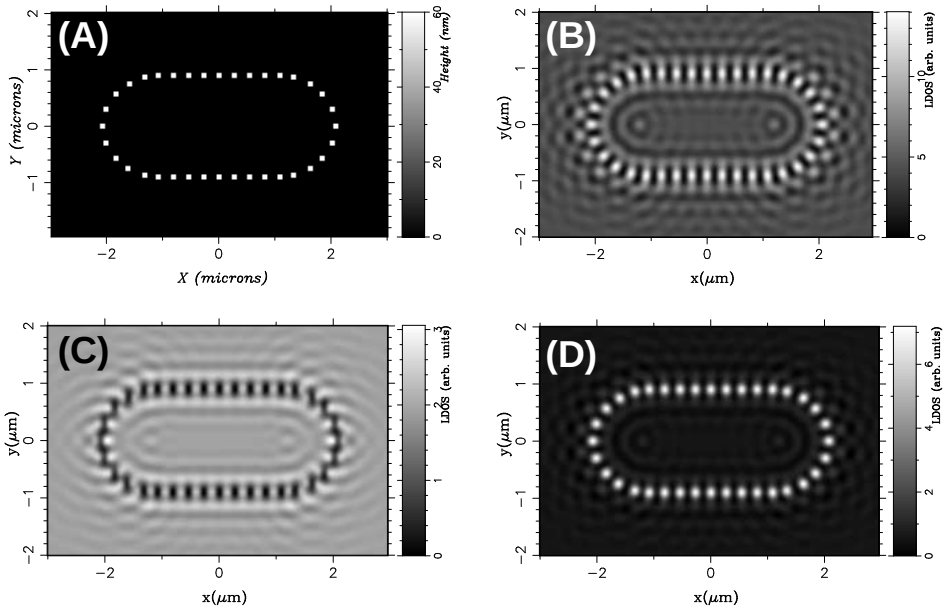

Figure 1. (A) Top view of the model structure. Glass pads (section 90×90 nm^2, height 60 nm) deposited on a flat glass substrate. At a constant height, 160 nm above the flat surface and for a wavelength in vacuum equal to 543 nm: (B) Electromagnetic LDOS; (C) Partial LDOS $\rho_{xx}(\mathbf{r}_m, \omega)$; (D) Partial LDOS $\rho_{zz}(\mathbf{r}_m, \omega)$.

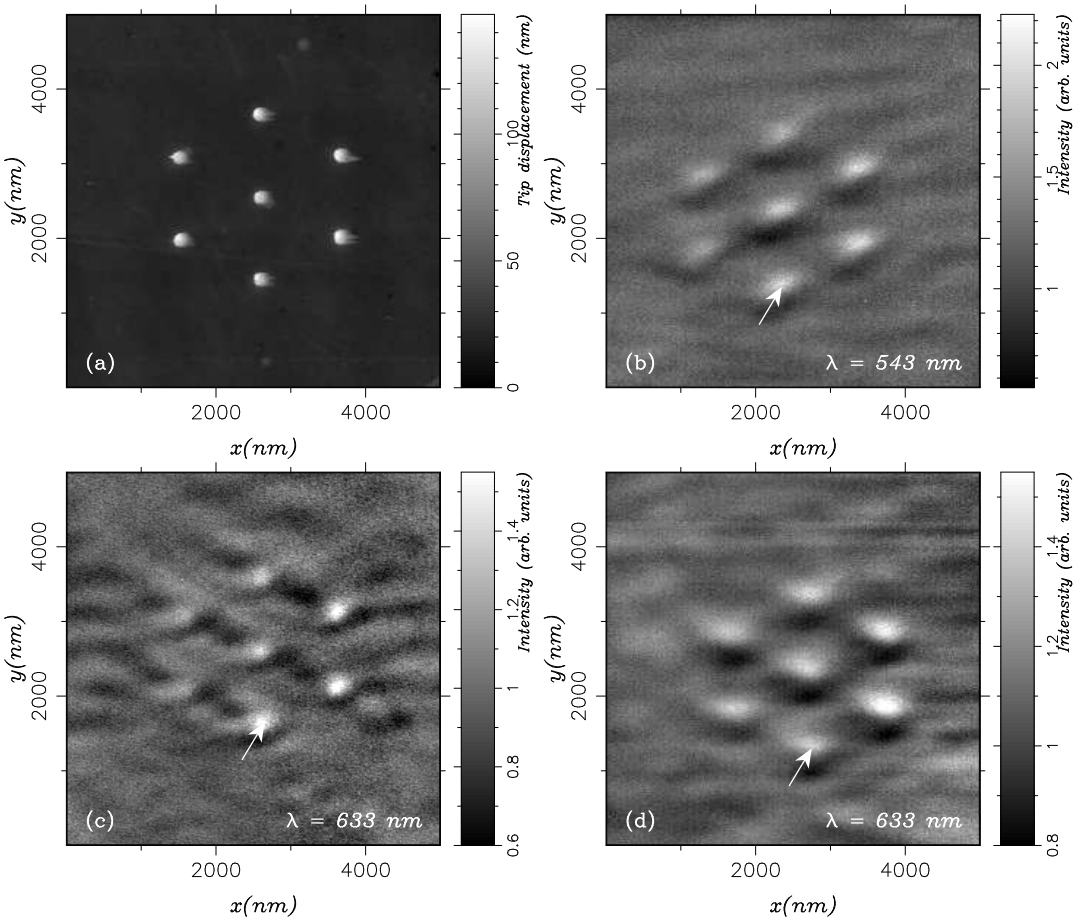

Figure 2. (a) AFM image of the sample. Tracks close to the pads along the scanning direction (x) are due to the presence of water on the sample. PSTM images recorded with dielectric tips: (b) $\lambda = 543$ nm; (d) $\lambda = 633$ nm. (c) PSTM image recorded with the semi–coated tip at $\lambda = 633$ nm.

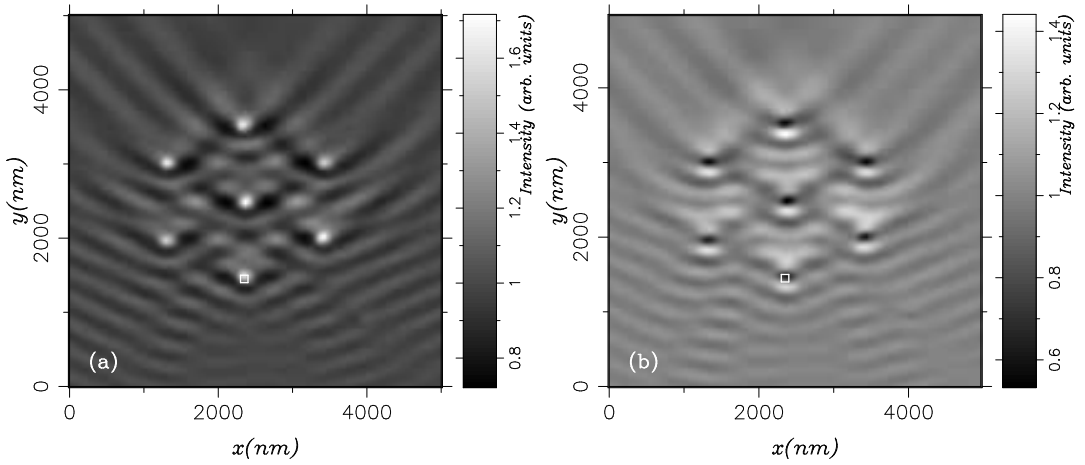

Figure 3. Theoretical near-field distributions (tip not included; TM polarized incident wave: $\lambda = 633$ nm, $\theta = 60$ degrees, $\psi = 90$ degrees) of the normalized electric $|\mathbf{E}(\mathbf{r})|^2$ (a) and magnetic $|\mathbf{H}(\mathbf{r})|^2$ (b) intensities close to the sample surface.

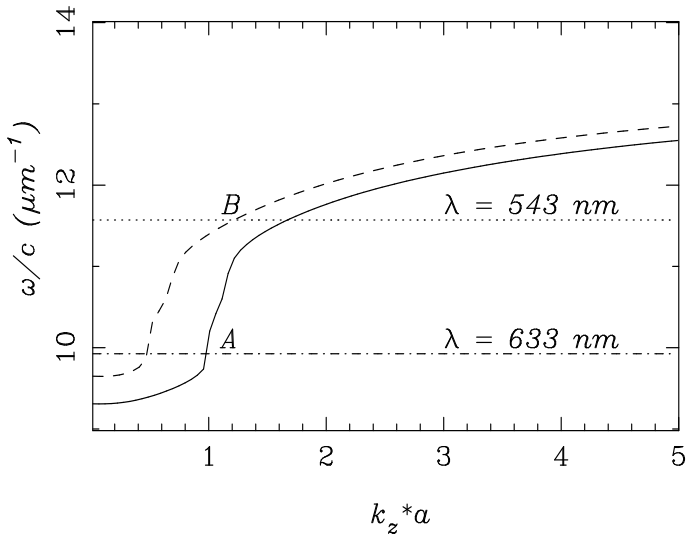

Figure 4. Dispersion curves of the $m = 1$ coated cylinder plasmon modes for the ratios $a/b = 1.3$ (solid line) and $a/b = 1.4$ (dashed line). k_z is the wavenumber along the longitudinal axis of the cylinder. The dot-dashed and dotted straight lines determine the two laser frequencies (here converted in units of wavelength in vacuum) operated in the experiments reported in this paper.

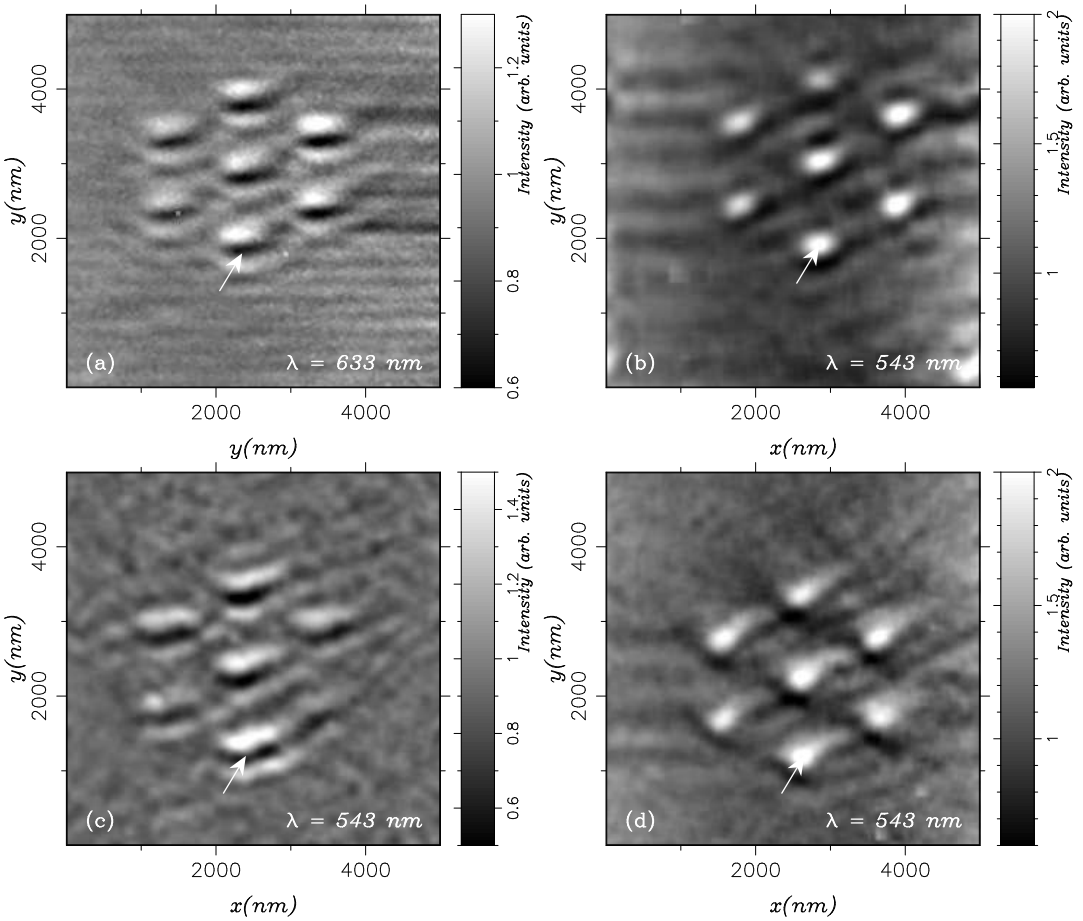

Figure 5. PSTM images recorded with Au coated tips: (a) $d = 20$ nm, $\lambda = 633$ nm; (b) $d = 20$ nm, $\lambda = 543$ nm; (c) $d = 30$ nm, $\lambda = 543$ nm; (d) $d = 35$ nm, $\lambda = 543$ nm.